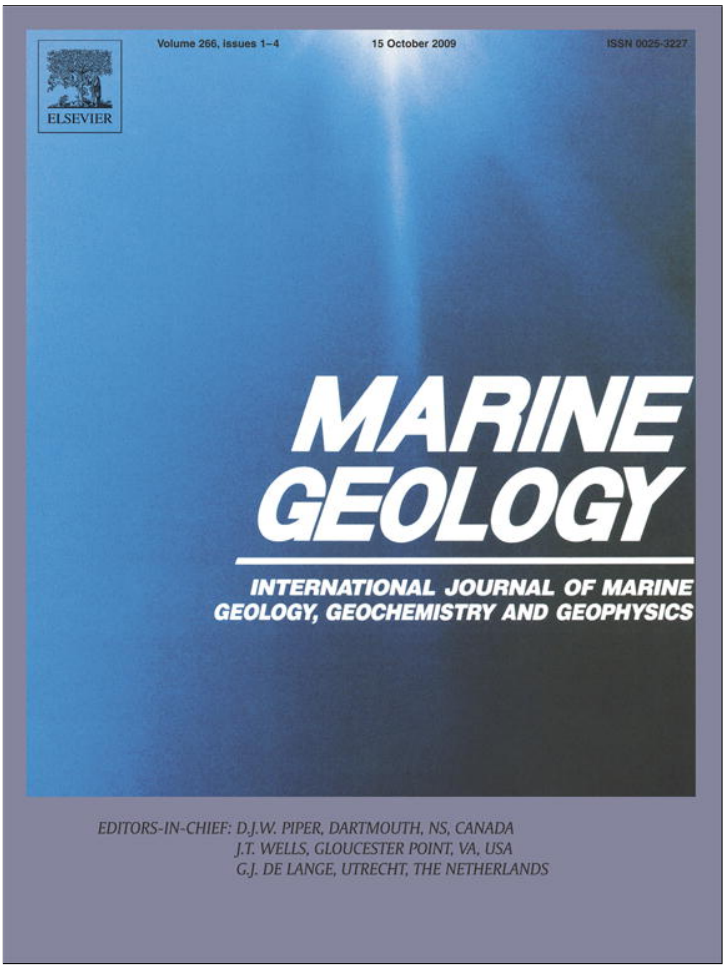

Marine Geology 266 (2009) 1–17

Contents lists available at ScienceDirect

Marine Geology

journal homepage: www.elsevier.com/locate/margeo

Pocket beach hydrodynamics: The example of four macrotidal beaches, Brittany, France

A. Dehouck [a,*], H. Dupuis [b], N. Sénéchal [b]

[a] Géomer, UMR 6554 LETG CNRS, Université de Bretagne Occidentale, Institut Universitaire Européen de la Mer, Technopôle Brest Iroise, 29280 Plouzané, France
[b] UMR 5805 EPOC CNRS, Université de Bordeaux, avenue des facultés, 33405 Talence cedex, France

ARTICLE INFO

Article history:
Received 24 February 2009
Received in revised form 6 July 2009
Accepted 10 July 2009
Available online 18 July 2009

Communicated by J.T. Wells

Keywords:
beach morphodynamics
embayed beach
beach cusps
rocky coast

ABSTRACT

During several field experiments, measurements of waves and currents as well as topographic surveys were conducted on four morphologically-contrasted macrotidal beaches along the rocky Iroise coastline in Brittany (France). These datasets provide new insight on the hydrodynamics of pocket beaches, which are rather poorly documented compared to wide and open beaches. The results notably highlight a cross-shore gradient in the magnitude of tidal currents which are relatively strong offshore of the beaches but are insignificant inshore. Despite the macrotidal setting, the hydrodynamics of these beaches are thus totally wave-driven in the intertidal zone. The crucial role of wind forcing is emphasized for both moderately and highly protected beaches, as this mechanism drives mean currents two to three times stronger than those due to more energetic swells when winds blow nearly parallel to the shoreline. Moreover, the mean alongshore current appears to be essentially wind-driven, wind waves being superimposed on shore-normal oceanic swells during storms, and variations in their magnitude being coherent with those of the wind direction. We also found evidence for the contribution of infragravity waves to the formation of an intertidal sand bar (through prolonged duration of swash processes at the same beach level) and to the development of beach cusps (but not to their initiation), for which the observed standing edge wave pattern may have been enhanced by the enclosed pocket-beach setting. The paper highlights some of the specificities of pocket beach with regards to their hydrodynamics and morphodynamics. More detailed observations would be needed, however, prior to a more comprehensive review.

1. Introduction

Small pocket beaches are constrained sedimentary systems, nested in between rocky headlands. They generally experience little or no sedimentary connection with one another because of headlands which regulate sand storages and transfers along the coastline. Although this type of beach is common worldwide along rocky coasts, documentation on their hydrodynamics, sediment transport processes and morphodynamics is sparse. Much of the scientific knowledge on inshore hydrodynamics concerns open beaches and the relevance, to pocket beaches, of various processes, such as bar formation (e.g., Wijnberg and Kroon, 2002; Masselink et al., 2006), and cusp generation (Inman and Guza, 1982; Werner and Fink, 1993; Coco et al., 2000), still needs to be addressed.

Since studies dealing with pocket beaches are rare, there is still significant scope for gaining further insight into the way their geomorphological and geological context (embayed setting, bounding headlands, rocky shoreface) may induce specificities in terms of the hydrodynamics, sediment transport and morphological behaviour. For example, Wright and Short (1984), Short (1991) and Horn (1993) reported observations from pocket beaches in Australia and along the Isle of Man coast in the Irish Sea that enabled them to classify the wide range of microtidal and macrotidal beach morphologies. Storlazzi and Jaffe (2002) found evidence for strong geological control of the hydrodynamics and sediment transport processes off a pocket beach along the rocky coast of central California. These authors showed that the direction of wave-induced flows and associated sediment fluxes in water depths of 12 m was a function of the inner shelf morphology, which comprises a palaeo-stream channel flanked by bedrock highs. Özkan-Haller et al. (2001) demonstrated discrete standing edge waves resulting from resonances related to the longshore beach width on a Spanish pocket beach, in contrast to the broad-banded edge wave field generally observed on open beaches (e.g. Oltman-Shay and Guza, 1987). This may lead to specific alongshore rhythmic patterns in the sand, for instance, beach cusps, rip channels and crescentic sand bars. However, Holman et al. (2006) and Turner et al. (2007) recently discussed rip-channel behaviour in both embayed and open settings and they found no evidence that alongshore edge waves were relevant to morphological evolution.

Given their confinement between headlands and the sheltered positions of some pocket beaches relative to oceanic swell, this type of beach may be expected to share common hydrodynamic characteristics

* Corresponding author. Present address: UMR 5805 EPOC CNRS, Université de Bordeaux, avenue des facultés, 33405 Talence cedex, France. Tel.: +33 5 40 00 29 61; fax: +33 5 56 84 08 48.
E-mail address: a.dehouck@epoc.u-bordeaux1.fr (A. Dehouck).

0025-3227/$ – see front matter © 2009 Elsevier B.V. All rights reserved.
doi:10.1016/j.margeo.2009.07.008

with those of embayed fetch-limited environments, examples of which have been documented by Jackson et al. (2002), Costas et al. (2005), Goodfellow and Stephenson (2005). Where incident swell waves are shore-normal, the longshore current is supposed to be very weak in the surf zone of a pocket beach unlike on open beaches (e.g., Thornton et al., 1996; Levoy et al., 2001; Anthony et al., 2004; Castelle et al., 2006a; Sedrati and Anthony, 2007). Nonetheless, a number of studies have also highlighted the important role of wind forcing in controlling nearshore and foreshore processes and beach morphological change (e.g., Pattiaratchi et al., 1997; Masselink and Pattiaratchi, 1998b; Sedrati and Anthony, 2007). As suggested by Özkan-Haller et al. (2001), infragravity waves are also expected to develop standing edge wave patterns, due to reflections on both sides of the beach, that could force the generation of rhythmic morphologies, such as beach cusps, that would "fit" the beach (Huntley and Bowen, 1978; Inman and Guza, 1982; Holman and Bowen, 1982). This is more likely than on open beaches where the self-organization hypothesis of cusp formation has found strong support (Werner and Fink, 1993; Coco et al., 2000; Falqués et al., 2000; Castelle et al., 2006b; Coco and Murray, 2007).

Although they may be in close proximity to each other, sometimes only separated by hundreds of metres, pocket beaches are rather singular environments that exhibit large variability in terms of wave exposure, grain size, beach slope and bedforms. In this paper, our objective is to report observations on the hydrodynamics of pocket beaches based on data collected along four morphologically-contrasting macrotidal beaches in the Iroise sea in Brittany (France). The area of interest is described in the next section, followed by data collection and processing methods. Results regarding beach morphological change and hydrodynamic processes observed during the field experiments are developed in Section 4, and discussed in Section 5. The extent to which the hydrodynamic signatures and morphodynamic behaviour of these beaches may also be similar to those of open beaches is also discussed.

2. Study area

2.1. Regional setting

The study area is the Iroise sea coastline located at the western end of Brittany, France (Fig. 1). The morphology of the shoreline includes seacliffs, small pocket beaches backed by cliffs or situated at stream mouths, and wide embayed beaches backed by sand dunes. Pocket beaches are nested in rocky bays delimited by tectonic faults of Hercynian

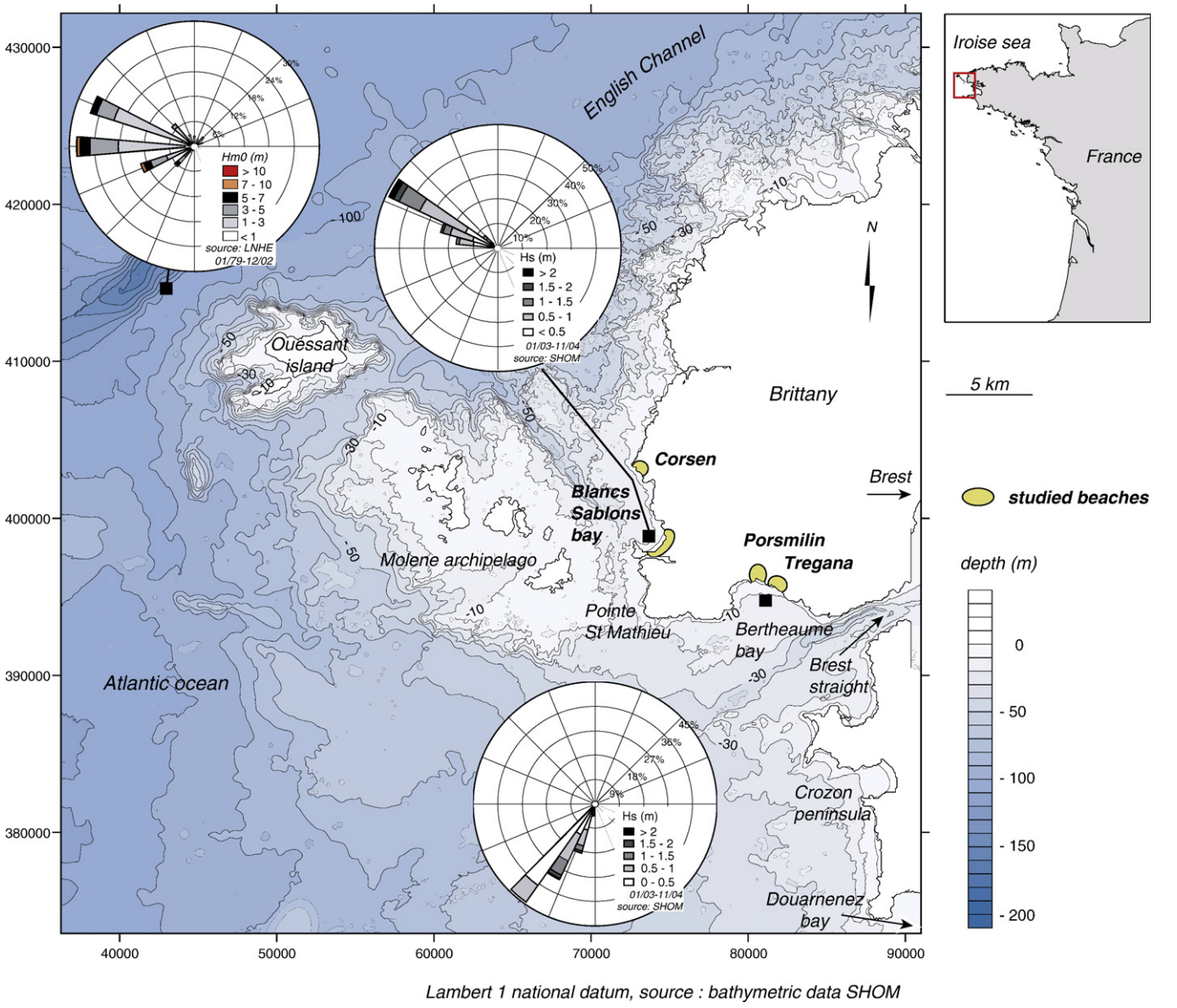

Fig. 1. Location map of the study area, bathymetric chart of the Iroise Sea (according to Lambert 1 datum) and wave roses offshore of the studied beaches.

heritage. Adjacent pocket beaches are separated from each other by headlands, cliffs and bedrocks extending offshore that obstruct the alongshore sand transport generated in the surf zone. Moreover, the intertidal zone of these pocket beaches is often bounded alongshore by a rocky seabed which sometimes extends down to the subtidal zone, forming a sort of natural groyne. Individual adjacent pocket beaches thus behave independently, with little sedimentary connection.

Tides are semi-diurnal and symmetrical, and the mean spring tidal range is 5.7 m (macrotidal). The mean speed of spring tidal currents is 0.4 and 0.7 m/s off the beaches, respectively in Bertheaume and Blancs Sablons bays (SHOM, 1994). The Iroise sea is a highly-energetic wave-dominated setting considering the annual and decadal significant wave heights of 11.3 m and 14.5 m offshore of Ouessant island in 110 m water depth (computed from a 23-yr sea state database supplied by the Laboratoire National d'Hydraulique et d'Environnement; see the wave rose in Fig. 1). Energetic swells originate from low and high pressure centres in the North East Atlantic Ocean. However, along this rocky coastline, wave propagation is considerably affected

Fig. 2. Photographs of the beaches, (a–b) the reflective pocket beaches of Corsen and Tregana, (c) the Low Tide Terrace Porsmilin Beach and (d) the dissipative embayed Blancs Sablons Beach.

by refraction and diffraction processes generated by the large continental shelf, headlands, shoals and islands located offshore of the beaches (Ouessant island, Molene archipelago). In spite a storm-dominated offshore wave climate, incident waves are highly dissipated, thus resulting in the moderate energy conditions on the pocket beaches. Storm waves are 0.8 to 1.5 m high while the mean annual wave height is less than 0.5 m (see offshore wave roses in Fig. 1). Pocket beaches are also commonly sheltered from storms due to coastal orientation. Hence, the oceanic swells that reach the shoreline have a quasi-normal incidence angle. Some of the beaches are also fetch-limited due to the protection offered by cliffs, headlands and even sometimes by the vicinity of adjacent, directly-facing stretches of coastline.

Bathymetric surveys offshore of Porsmilin Beach have shown that the rocky seabed crops out at a depth of −3 m (below the Lowest Astronomical Tide Level, noted LATL hereafter), suggesting a limited cross-shore extent of the beach sedimentary prism (Dehouck et al., 2007). The closure depth (Hallermeier, 1981) computed using a 2-yr (2003–04) sea-state dataset obtained offshore of the beaches (run by the Service Hydrographique et Océanographique de la Marine) lies between −3.4 m and −4.5 m along the study area, in close agreement with the moderate wave energy context, and as confirmed by the surveys.

2.2. Field sites

The study focuses on four different sites (Fig. 2): three small pocket beaches and a wider (1-km long) embayed beach, chosen for the variety of their morphologies (slopes, bedforms), sediment grain sizes and wave exposures (Table 1). In fact, beach types range from purely reflective (Corsen and Tregana beaches), through the Low Tide Terrace type (Porsmilin Beach), to featureless ultra-dissipative (Blancs Sablons Beach), according to the Masselink and Short (1993) classification. Swash bars formed at stationary water levels are occasionally present in the intertidal zone at Porsmilin and Tregana beaches, developing parallel to the shoreline with little alongshore variability. Their trough-to-crest height ranges from about 10 cm for sand bars developing at the spring low tide level up to 1 m for those located at the neap high tide level. In the latter case, a landward sand bar migration may occur under favourable persistent low-energy conditions and rising neap-to-spring tidal range, culminating in the formation of a berm. Rhythmic beach cusps are also widely present on the beaches, sometimes as permanent features (Tregana Beach) but most of the time as temporary ones.

Sediments are fine to coarse sands in the intertidal zone with a median grain size (d_{50}) that gets larger on steep beaches (Table 1). Samples collected across the beachface show a cross-shore variability of the median grain size mainly due to coarser sediments around the crest of intertidal bars ($d_{50}\approx0.7$ mm), beach cusp horns and in exfiltration channels ($d_{50}\approx3$ mm). However, no detailed information is available on the longshore distribution of the sediment size.

Table 1
Main characteristics of the field sites.

	Blancs Sablons	Porsmilin	Tregana	Corsen
Median grain size (μm)	250	320	370	450
Intertidal zone width	300	200	100	50
Morphological patterns (shoreface)	–	Temporary swash bars and beach cusps	Temporary swash bar and permanent beach cusps	Temporary beach cusps
Shoreface slope	0.02	0.05–0.08 (*u) 0.02–0.035 (*l)	0.09	0.12
Beach type	Dissipative	Low tide terrace	Reflective	Teflective
Shore-normal wave direction	NW	S	S	WSW
Backshore	Large sand dunes	Seawall/remanent sandy scree	Seawall/soft cliff	Rocky cliff

*u and *l are abbreviations for upper and lower beach.

Table 2
Characteristics of sensor deployment.

	Blancs Sablons	Porsmilin	Corsen	Tregana
Experiment duration	5 weeks	4 weeks	2 weeks	1 week
Burst duration	30 min every 60 min	20 min every 30 min	10 min every 30 min	10 min every 30 min
Sensor height (m)	+0.45	+0.45	+0.55	+0.55
Sensor location	Subtidal zone (−6 m)	Lower intertidal zone (+1.5 m)	Lower intertidal zone (+1.7 m)	Lower intertidal zone (+2.6 m) then upper intertidal zone

Depth are in meters according to the national hydrographic datum (where zero level is the Lowest Astronomical Tide Level).

3. Materials and methods

3.1. Field data

3.1.1. Data sampling strategy

Field experiments were performed for one to five weeks in spring 2004 and 2005 on the four beaches. Wave and current measurements

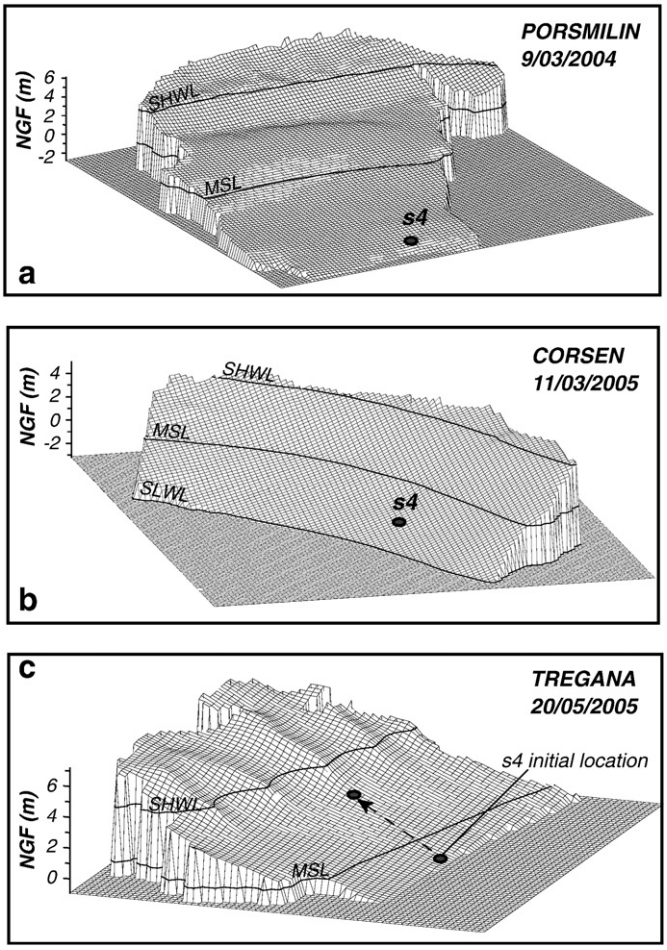

Fig. 3. Intertidal beach topography at the beginning of the field experiments and sensor locations across the three pocket beaches. MSL, SHWL, SLWL indicates mean sea level, spring high water line and spring low water line (the latter only figuring on Fig. 3b as the intertidal topography was not fully surveyed on the other beaches) relative to the national elevation datum (NGF).

Table 3
Tide and wave conditions during field experiments.

	Blancs Sablons	Porsmilin	Corsen	Tregana
Tidal range (m)	1.3–6.5	1.3–6.5	1.3–6.9	3.5–5.6
Wave height H_s (m)	0.1–1.5	0.1–1.3	0.1–0.8	0.4–1.6
Significant period $T_{1/3}$ (s)	6.4–14.9	4.1–18.5	3.6–18.9	5.4–13.0
Mean period $\overline{T_{1/3}}$ (s)	10.8	11.4	10.5	8.9

were recorded with electromagnetic (S4DW InterOcean systems) and acoustic current meters (ADV Nortek) deployed in bottom-mounted frames. Only the electromagnetic current meter data are analyzed in this paper (Table 2). Data were obtained at a frequency of 2 Hz in bursts of 10 to 20 min every 30 min. Sensors were initially located 45 to 55 cm above the sea bed in the lower intertidal zone for three of the four beaches and in the subtidal zone at Blancs Sablons beach (to prevent surfers from being hurt, and damage to the sensors).

Topographic surveys were realized during daylight hours at low tide, every day during the one week-long experiment and every few days during longer experiments (optimizing surveys during spring tides), using a DGPS (Trimble 5800). The initial beach state and location of the sensors are shown in Fig. 3 (elevations relative to the national geographic datum "Nivellement Géographique Français", basically the Mean Sea Level).

Wind information (10-min average speed and direction at 6 am, 12 am, 6 pm) was collected at the local wind station of Meteo France located at Pointe St Mathieu (Fig. 1) a few kilometres, from the four sites.

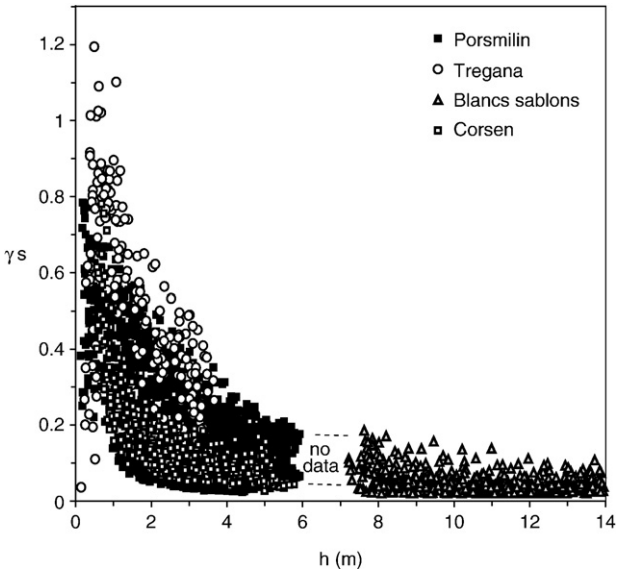

Fig. 5. The relative wave height versus water depth for all wave conditions at the four field sites.

3.1.2. Offshore conditions during field experiments

The experiments were designed to cover various wave and tide conditions and to assess wave action during both high-energy events and calm periods (Table 3). Instruments were deployed at least during a neap-spring tidal cycle. For instance, two depressions off Ireland (19/3/04) and Brittany (31/3/04) generated large swells (H_s = 3–7 m off Ouessant) and strong winds (>10 m/s) for several days (storms D and E ; Fig. 4a), winds turning clockwise from the S to the N while the depressions were moving towards northern Europe. These events produced significant wave heights of 1.3 m at Porsmilin Beach (Fig. 4b). As a general rule, the level of wave energy on the beaches is consistent with the occurrence of strong local onshore winds superimposed on large-fetch swells.

3.1.3. Morphological observations

At the beginning of the experiment, Porsmilin Beach was characterized by beach cusps in the upper foreshore, a rectilinear intertidal sand bar at neap high tide levels and a dissipative low tide terrace (Fig. 3a). The main morphological changes occurred shortly after the beginning of the experiment whilst the cusps and the sand bar were eroded by storms A and D (Fig. 4b). Then, two episodes of sand bar formation at the spring low tide level were recorded after storms D and E. Corsen Beach was characterized by a steep foreshore slope (Fig. 3b). A wide and well-developed beach cusp system was present across the upper foreshore at

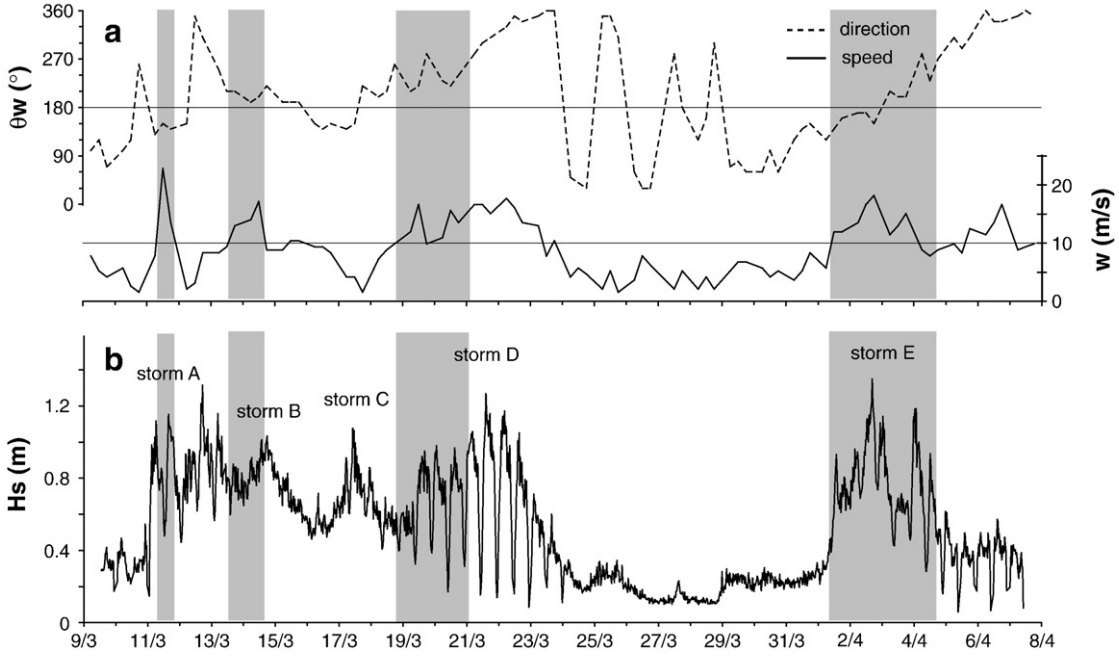

Fig. 4. Wind and wave conditions at Porsmilin Beach (a) mean wind direction θ_w and wind speed w; (c) significant wave height H_s. Grey bars highlight periods of stormy near-onshore winds.

Tregana Beach (Fig. 3c). A full life-cycle of beach cusps was observed with their partial destruction, the initiation and the development of a new cusp system.

3.2. Data processing

Time series of flow speed and flow direction were processed into mean cross-shore (U) and longshore (V) currents averaged over the burst duration (Table 2). Sea surface elevation data were corrected to account for tidal fluctuations, sensor height and atmospheric pressure variations. First, data recorded while the sensor was out of water were removed by arbitrarily selecting all bursts during which elevation fluctuations were less than 2 cm. The raw signal was then detrended for each burst duration to remove tidal fluctuations and corrected to account for burying and erosion at the frame foot.

Sea surface elevation time series were processed in the spectral domain with a Fast Fourier Transform of 50% overlapping Hanning-windowed data segments averaged over the burst duration (dof = 6). Herein, separations between far infragravity waves, infragravity waves, gravity waves and turbulence were defined at respective frequencies of 0.01 Hz, 0.05 Hz (low frequency cut-off) and 0.5 Hz (high frequency cut-off). The significant wave height (H_s) was computed as four times the zero spectral moment integrated over the 0.05–0.5 Hz band.

Hydrodynamic processes associated with each morphodynamic zone were analyzed using the significant wave height H_s to water depth h ratio ($\gamma_s = H_s/h$) consistent with previous studies (e.g. Masselink, 1993; Kroon and Masselink, 2002; Masselink et al., 2006; Price and Ruessink, 2008). A complete dataset embracing shoaling to inner surf zone conditions was obtained (Fig. 5) that permitted separation of the different morphodynamic zones i.e., breaking conditions in the surf zone from non-breaking conditions in the shoaling zone. The increase in relative wave height H_s/h is shown as a function of depth, from nearly 0 up to 1.2 due to wave energy dissipation across the surf zone (Osborne and Greenwood, 1992; Ruessink et al., 1998). This range of values is consistent with former observations gathered on open beaches (Raubenheimer et al., 1996; Sénéchal et al., 2001, 2005).

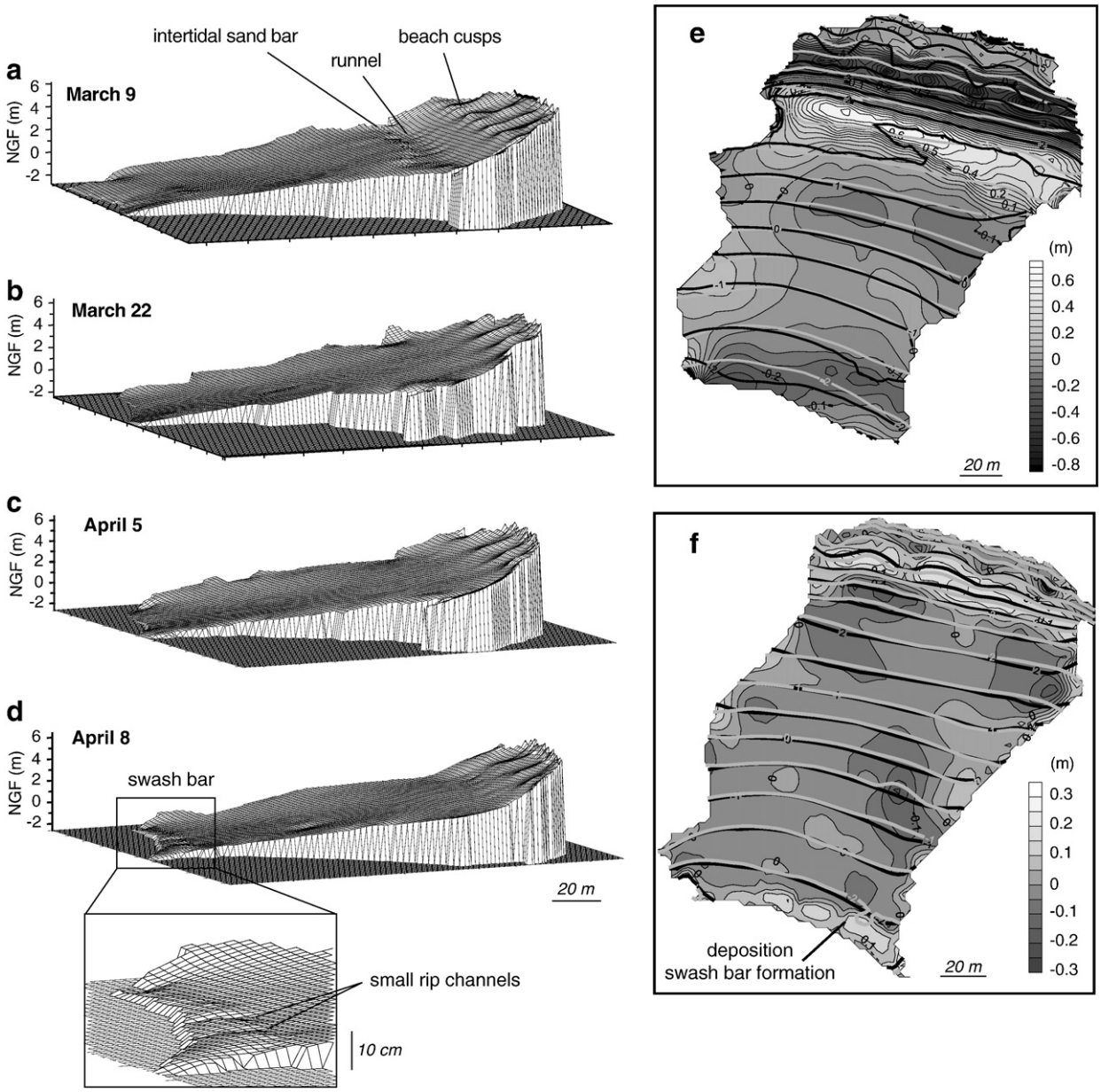

Fig. 6. (a–d) Porsmilin Beach topography on March 9, 2004, March 22, April 5, April 8; (e–f) elevation change in metres between March 9–22 and April 5–8 surveys (coloured contours) with the topographic lines superimposed in black (antecedent) and grey (final topography). Elevations are relative to NGF datum.

Non-linear wave interactions in shallow waters were investigated by computing bispectra of the sea surface elevation time series (25% overlapping windows of 4 min). They were used to highlight the nature of the observed high frequency waves, i.e., bound waves forced by the incident wave group or wind waves locally generated. We focused on the bicoherence (b^2 (f_1; f_2)) which gives an indication of the relative degree of phase coupling between triad of waves (f_1, f_2, $f_3 = f_1 \pm f_2$) with $b = 0$ for random phase relationships and $b = 1$ for a maximum amount of coupling (Kim and Powers, 1979).

Cospectra of the sea surface elevation and flow speed time series were also computed over a defined frequency band to determine the progressive or standing nature of the observed infragravity waves. If both signals are well-correlated and in phase ($\varphi = 0$), the infragravity wave is progressive while standing if signals are out of phase ($\varphi = \pm\pi/2$) (Huntley and Bowen, 1978; Oltman-Shay and Guza, 1987).

Finally, processes involved in beach cusp formation were explored by testing the two main theories commonly admitted, and implicating (1) a standing edge wave (Guza and Inman, 1975), and/or (2) self-organization (Werner and Fink, 1993; Coco et al., 2000). Predicted beach cusp wavelength (L_c) according to the standing edge wave theory is given by Eqs. (1) and (2) (assuming "mode zero" edge waves), while, according to self-organization theory, by Eq. (3).

For a subharmonic wave, $$L_c = L_{e(sh)} / 2 = (g/\pi) T_p^2 \tan\beta \quad (1)$$

for a synchronous wave, $$L_c = L_{e(sy)} = (g/2\pi) T_p^2 \tan\beta \quad (2)$$

with L_e being the edge wavelength, T_p the spectral peak period and $\tan\beta$ the beach slope.

$$L_c = FS \quad (3)$$

where F is an empirical constant equal to 1.7 (Werner and Fink, 1993), S the cross-shore swash length defined as the ratio of the breaking wave height to the swash zone slope ($H_b/\tan\beta_{swash}$), where H_b is assumed similar to H_s. Some details of how the run-up height becomes a function of the breaking wave height can be found in Baldock and Holmes (1999).

4. Results

4.1. Beach morphological change

4.1.1. Intertidal sand bars

Morphological change at Porsmilin Beach focused on the behaviour of intertidal sand bars, the one present on March 9 at high tide levels (Fig. 6a) disappearing following to several high energy events, while another sand bar appeared later at low tide levels. The initial topography, characterized by a 70 cm-high sand bar, changed rapidly, notably the upper foreshore where the sand bar and cusps were subject to durably high wave energy conditions for 11 days (storms A–D) under spring tides. Beach cusps located around +4 m NGF were erased (20–80 cm of erosion at this level) while the runnel of the sand bar was filled up with 20–70 cm of sediment (Fig. 6e). In contrast, the mid-beach only suffered from minor erosion (<10 cm) as the beach

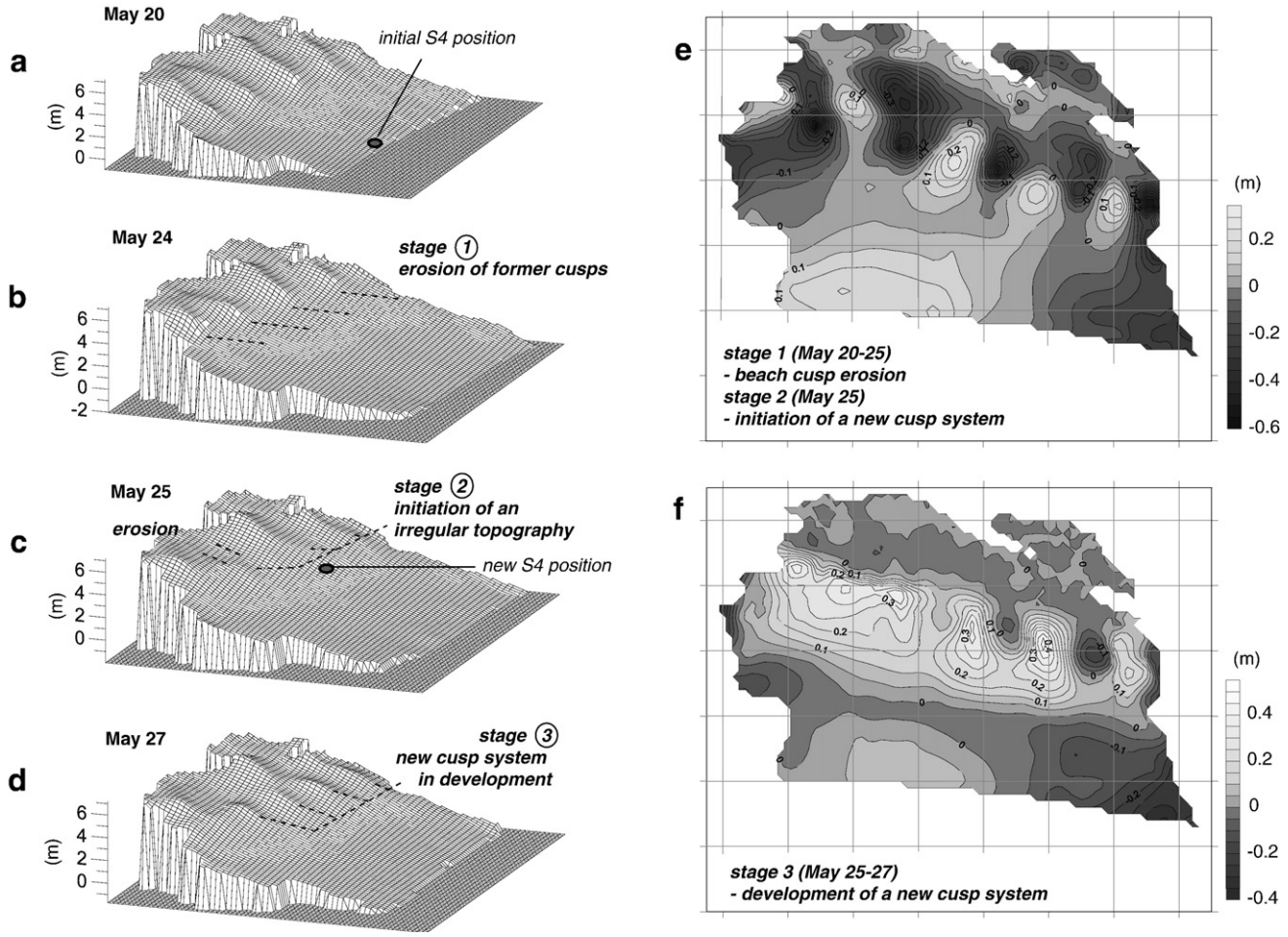

Fig. 7. (a–d) Tregana Beach topography on May 20, 2005, May 24, May 25, May 27; (e–f) elevation change in metres between May 20–25 surveys (erosion of former cusps and initiation of new cusps) and May 25–27 surveys (cusp development). Elevations are relative to NGF datum.

profile was already close to equilibrium before the storms. Some irregularities in the topography of the lower intertidal zone were smoothed. As the energy level began to weaken after storm D, the morphology evolved to that of a flat beach profile on March 22 (Fig. 6b).

Following this, two sets of observations showed the growth of an intertidal sand bar at the spring low tide levels associated with post-storm energy conditions. On March 26, bar formation began with a subdued bump observed at the eastern lower corner of the beach around −2 m NGF (not shown) that rapidly disappeared from sight as the tidal range decreased. The second event occurred as soon as moderate wave conditions resumed after storm E (April 5–8). A 10-cm high sand bar formed roughly at the same beach level, indented by small drainage channels (Fig. 6d). The rest of the beach remained mostly unchanged after March 22, notwithstanding the fact that the upper foreshore experienced moderate accretion during periods of low energy (Fig. 6f).

4.1.2. Beach cusps

At the beginning of the experiment, Tregana Beach was characterized by a system of five cusps with a mean spacing of 28 m extending widely across the upper foreshore from +2.5 to +6 m NGF (Fig. 7a). As the tidal range increased and the water level attained the cusps, progressive erosion set in, due to onshore wind waves (H_s = 0.8–1.4 m) affecting the horns around +3–4 m NGF (Fig. 7b). The storm peak (H_s = 1.6 m) occurred in the evening of May 24 and led to the total disappearance of one cusp located at +4.5–5 m NGF, whereas the other cusps only underwent moderate adjustments (Fig. 7c). This energetic episode caused significant erosion of the cusp system, 30–60 cm at the horns and 10 cm in the embayments (dark areas in Fig. 7e). Immediately after the storm peak in the early morning of May 25, three irregularly-shaped bumps emerged around +3–3.5 m NGF (Fig. 7c) associated with 20–40 cm of sediment deposition (clear patches in Fig. 7e). The incipient topography then developed during the following tides with bumps growing by 20 cm a day, finally evolving into four regular cusps on May 27 spaced 23.5 m on average (Fig. 7d). The initiation and development phases resulted in an overall accretion of 40–60 cm at the horns of the new cusps and little erosion in their embayments (Fig. 7f).

4.2. Hydrodynamics

4.2.1. Tidal currents

Data collected at Blancs Sablons Beach representative of non-breaking conditions (Fig. 5) are used to characterize tidal currents in the subtidal zone (7–14 m water depth) since these currents are known to be relatively strong offshore of the beaches (see Section 2). On this embayed beach, tidal currents are alternatively directed to the west around high tide and to the east around low tide water levels (Fig. 8). The magnitude of tidal currents is maximum during spring tides (Fig. 8a), ebb and flood mean currents reaching respectively 0.1 and 0.25 m/s (Fig. 9c). At the semi-diurnal time-scale (Fig. 8b), tidal currents reverse from east (ebb) to west (flood) around the mid-rising tide (LT + 3 h), and inversely one hour after high tide. The weak ebb current is maximum one to two hours after low tide, followed a few hours later by a peak in flood velocity near high tide level (from LT + 4 to HT). The strongest onshore-directed currents (U>0.05 m/s, underlined by grey bars in Fig. 9d) are not generated by spring ebb currents but are due to the combination of spring low tide levels and energetic swell conditions (Fig. 9a, b). During these two storm events, horizontal currents are no longer modulated by the tidal range alone but also by the incident wave forcing (H_s = 1.6 m on March 22 and 0.8 m on April 6). Therefore, skewed waves drive a significant onshore-directed flow component near the seabed, independently of the water level, even in water depths of 7–14 m. In addition, energetic swells contribute to counter-balance the offshore-directed flood while enhancing the ebb current in the onshore direction (Fig. 9 panels c–e), these effects being reinforced shoreward in shallower waters.

4.2.2. Wave-induced currents

As an indicator of wave energy dissipation across the surf zone, the relative wave height H_s/h serves to describe the space and time variability of wave-induced currents during the tidal cycle. It is shown in Fig. 10 as a function of the cross-shore and longshore mean currents (10- or 20-min average). Datasets obtained from the sensors located in the intertidal zone of the three pocket beaches are organized into two groups, the structure of which may lack clarity depending on the beach and the morphology considered. In fact, at Porsmilin Beach the low tide dissipative terrace is ideal for the observation of the suite of hydrodynamic processes in the intertidal zone (wave shoaling, surf,

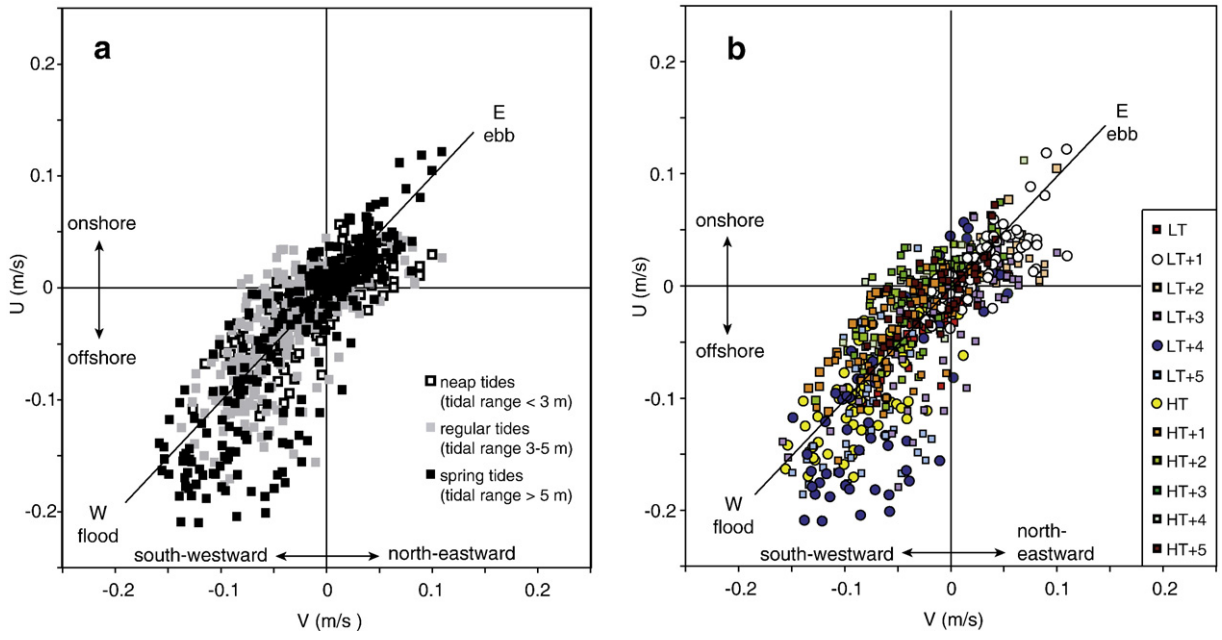

Fig. 8. Tidal currents at Blancs Sablons subtidal beach according to (a) the spring-neap tidal cycle, (b) the semi-diurnal tidal cycle. U, V stands for cross-shore and longshore flow components, LT and HT for low tide and high tide.

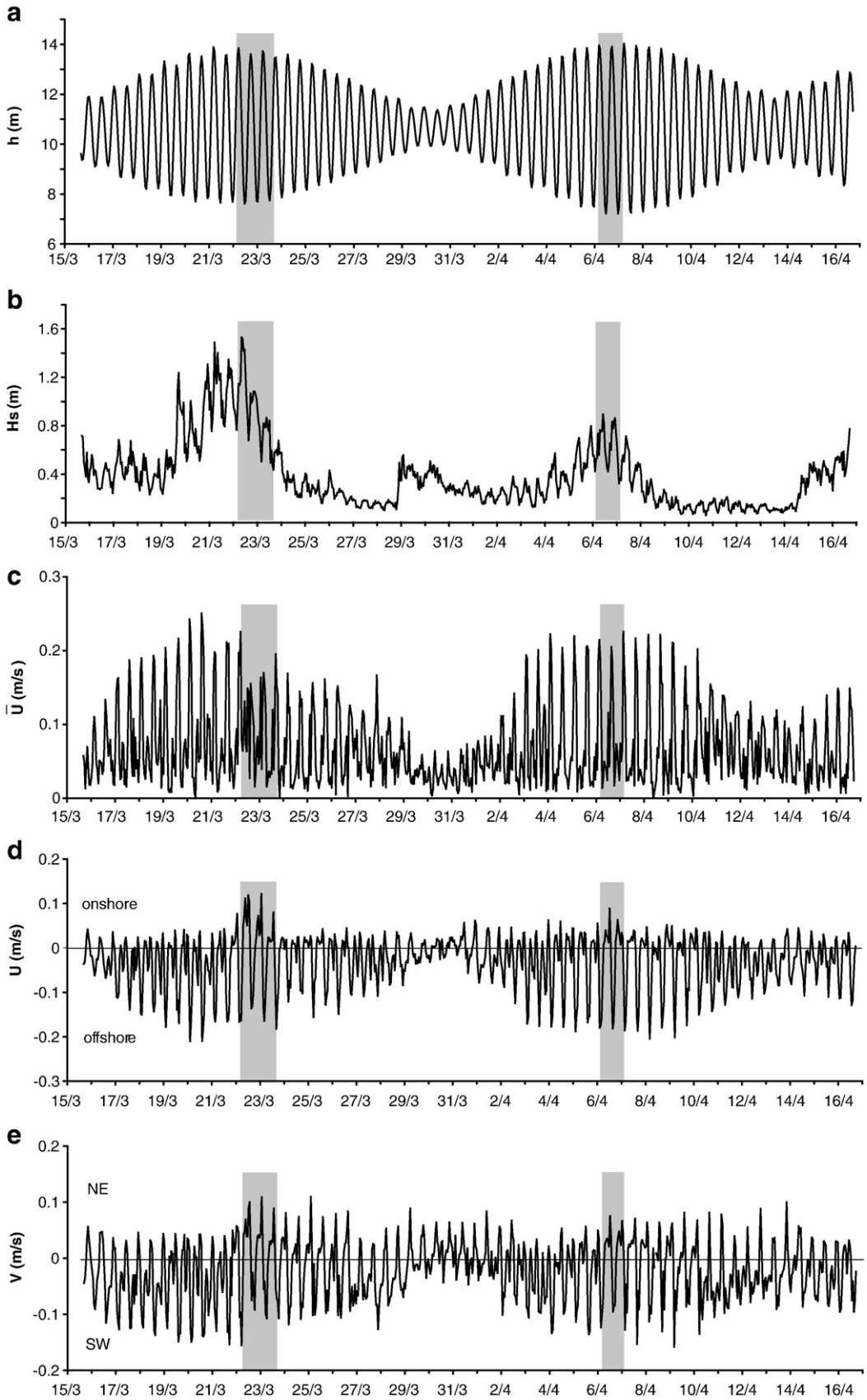

Fig. 9. Time series of water depth h, significant wave height H_s, mean flow speed $\bar{U}$, mean cross-shore U and longshore V flow speeds at the Blancs Sablons embayed beach (sensor located 6 m below LATL). Grey bars indicate the occurrence of an onshore-directed current component induced by skewed waves.

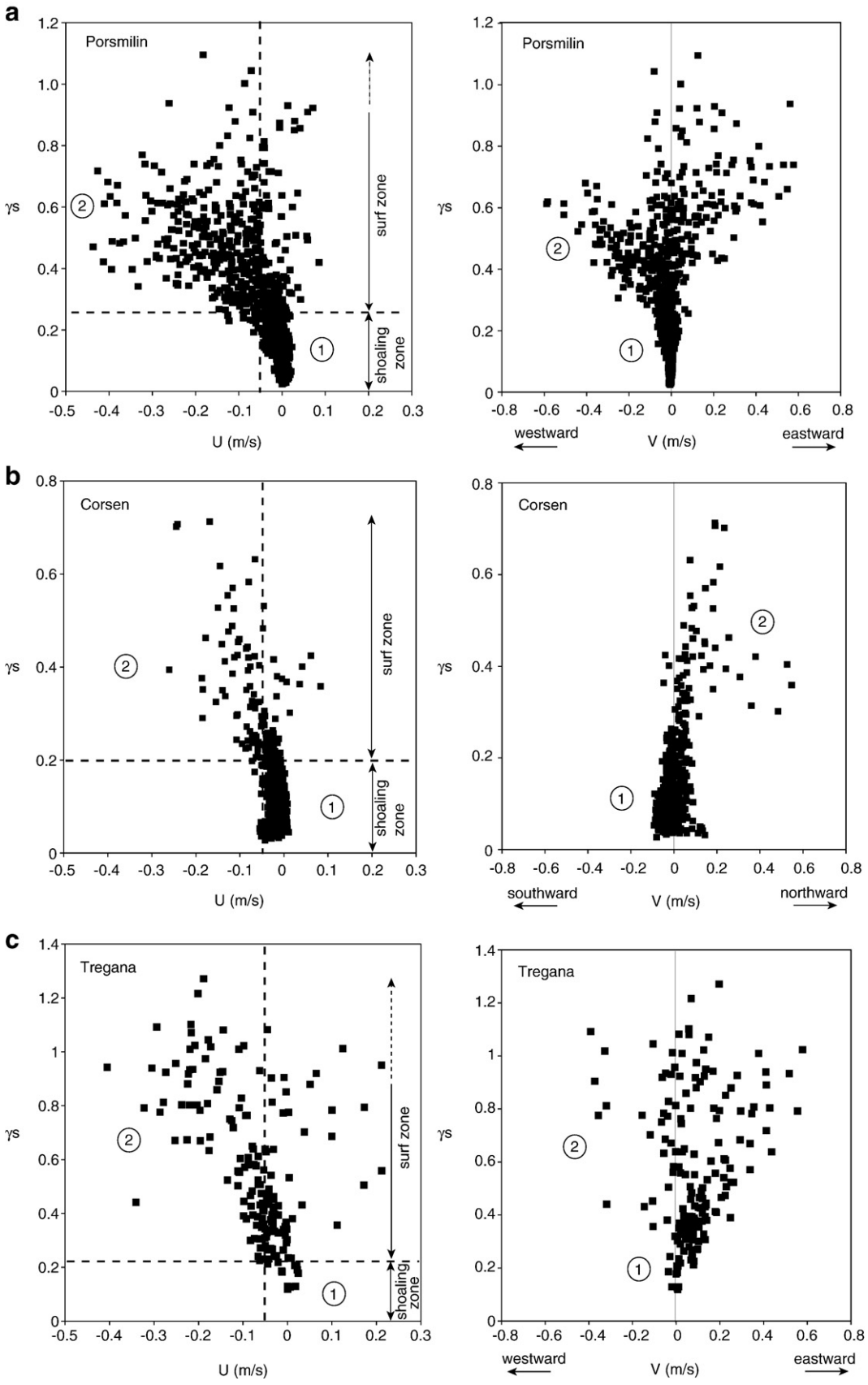

Fig. 10. The relative wave height versus the mean cross-shore and longshore flow speed as measured in the lower intertidal zone at (a) Porsmilin, (b) Corsen and (c) Tregana beaches. Negative (positive) values of cross-shore flow are for offshore (onshore)-directed flow.

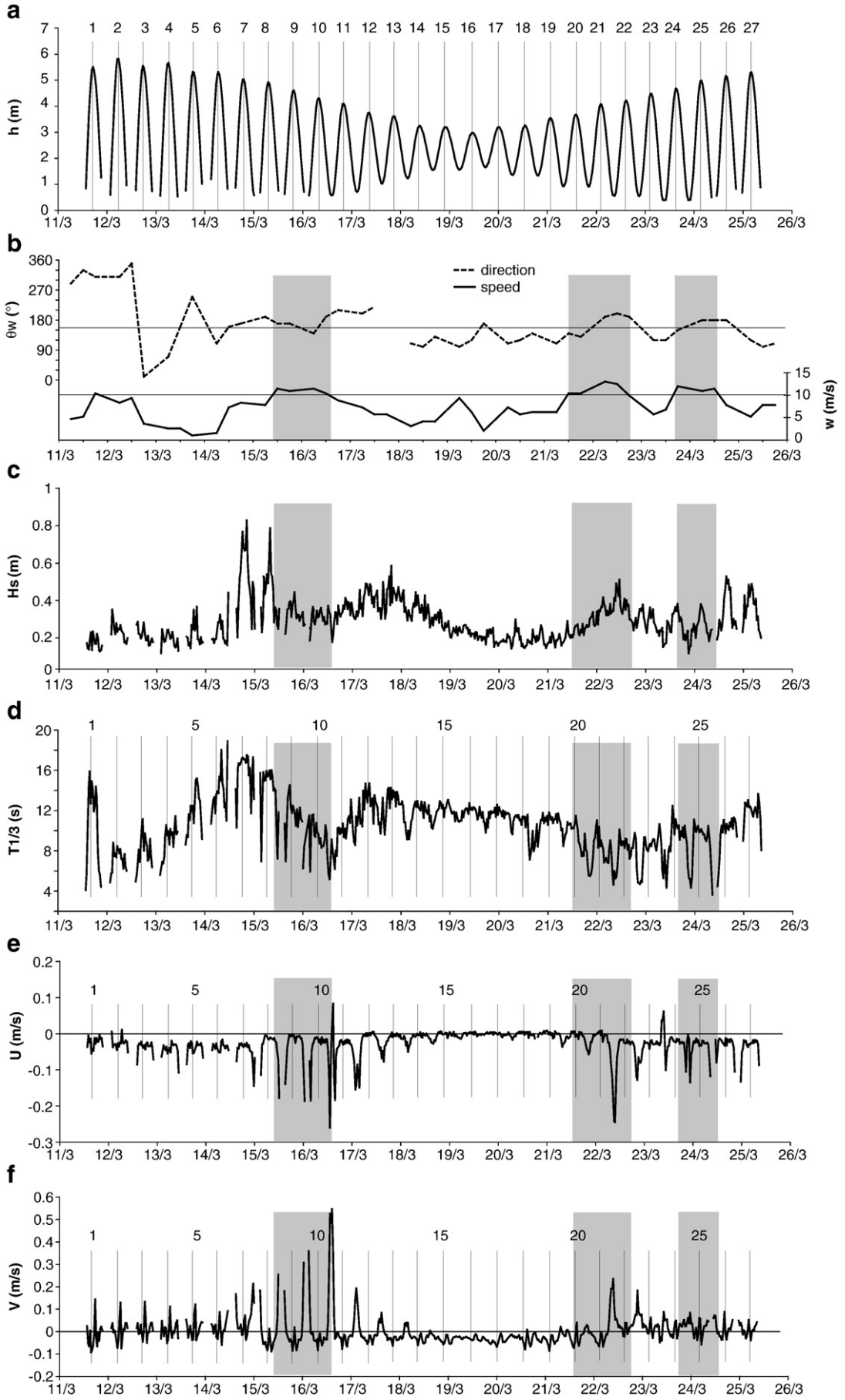

Fig. 11. Time series of water depth h, mean wind speed w and wind direction θ_w (solid line is for a shore-parallel wind direction), significant wave height H_s, significant wave period T1/3, mean cross-shore U and longshore V flow speed (V positive northward) at Corsen Beach. Grey bars indicate times of wind events (w>10 m/s).

swash), while on reflective beaches (i.e., Corsen, Tregana), the narrow surf zones and the occurrence of numerous processes within a few metres only induce more complexity in the following analysis.

Data from the first group (stated "1") were measured in the shoaling zone for weak relative wave heights associated with non-significant flow speeds (U and $V<0.05$ m/s). These values of H_s/h are low, all below 0.2 on average, and are thus representative of non-breaking conditions, as illustrated by the Blancs Sablons dataset (Fig. 5), the sensor of which was located in 7–14 m water depth and did not experience breaking. Hence, during calm periods (non breaking conditions), the mean flow speed is nearly zero whatever the time of the tidal cycle, suggesting that tidal currents are not significant in the intertidal zone of these pocket beaches.

The second group (stated "2") encompasses surf zone conditions with an observed near-bed offshore-directed current (the undertow) and intermediate relative wave heights. A negative cross-shore flow speed of 0.05 m/s is set as an arbitrary threshold value (vertical dashed line on Fig. 10) beyond which the offshore-directed flow becomes significant. Based on the assumption that the undertow velocity is minimum at the start of the surf zone (note that this point may be subject to controversy according to Masselink and Black, 1995), the H_s/h value associated with this threshold value separates non-breaking conditions in the shoaling zone from breaking conditions in the surf zone. It is a local and empirical breaking criterion that takes non-dimensional $(H_s/h)_b$ values from 0.2 to 0.25. These values are smaller than others gathered on open beaches where the start of the surf zone is commonly set around $H_s/h=0.3$–0.4 (van Enckevort and Reincke, 1996; Ruessink et al., 1998; Aagaard et al., 2002; Kroon and Masselink, 2002; Masselink et al., 2006) even though Price and Ruessink (2008) have recently argued that fixed values of H_s/h are not appropriate for separating shoaling and surf zones, but that this criterion depends on the local wave steepness (H_s/L). The undertow attains a mean speed of 0.25–0.45 m/s in the surf zone ($H_s/h=0.4$–0.8), this time in the range of commonly reported values of 0.2–0.3 m/s (Greenwood and Osborne, 1990; Masselink and Black, 1995; Masselink and Pattiaratchi, 1998b; Anthony et al., 2004), and up to 0.4 m/s on barred beaches (Garcez Faria et al., 2000; Aagaard et al., 2005). In the surf zone, a longshore current is observed with a mean speed up to 0.6 m/s and with a direction coherent with the incident wave propagation direction. During the experiments at Tregana and Corsen beaches, energetic events were characterized by a mixture of North-Atlantic swells and superimposed sea waves generated by local winds blowing several hours to days consecutively from the same direction at an incidence angle of 20 to 45° and even 70° at Corsen Beach (winds nearly parallel to the shoreline). This explains the trend of an almost uniformly-directed longshore flow to the north and to the east in the surf zone of Corsen and Tregana beaches respectively.

The highest relative wave heights (γ_s tending to 1) were also measured in the surf zone but closer to the swash zone. There, two wave-induced processes are in competition, the onshore surface mass transport induced by the skewed surf bores is balanced by the near-bed offshore-directed undertow. Depending on the water depth, and thus on the relative contribution of the undertow and surf bores, the cross-shore flow might still be directed offshore but weakened (undertow is the dominant process), or may reverse onshore (surf bores are dominant), while the longshore flow is hinged on the wave propagation direction. At this stage, it does not seem obvious to use fixed values of H_s/h to separate the two different sub-morphodynamic zones.

4.2.3. Wind forcing

Variations of the wave energy level at Porsmilin Beach were shown to be relatively consistent with the local wind forcing (see Section 3.1.) suggesting wind is a decisive factor controlling pocket beach hydrodynamics. The storm event D was particularly relevant regarding the decrease in wave energy that started on March 22 as soon as winds turned from the SW–W to the N (Fig. 4) while the offshore energy level and direction of incident swells were mostly unchanged. The response of the mean currents was immediate; the cross-shore flow velocity dropped by a factor of two between March 19–21 (0.2–0.3 m/s) and March 22 (0.1–0.15 m/s) (not shown). Moreover, the strong longshore flow directed to the E under SW winds decreased from 0.5 to 0.2 m/s on March 20 since the influence of wind forcing on the foreshore was considerably lessened for configurations of wind blowing from the W (albeit theoretically parallel to the shoreline but in the shadow of a cliff) until being almost nil for winds from the N. The shift from wind to swell-dominated conditions is shown by the gradual increase in the significant wave period from 11 s at the onset of storm D to 14 s during waning storm conditions.

Another change in wave forcing was recorded on March 15 at Corsen Beach, from long moderately energetic swells ($T_s=16$ s, $H_s=0.8$ m at tide 7) to wind-sea waves ($T_s=8$ s, $H_s=0.3$ m at tide 10) (Fig. 11 panels c,d). Mean flows were maxima during gale events from the S and SW (Fig. 11b), the undertow reaching 0.25 m/s and the longshore current flowing to the N at a mean speed of 0.5 m/s (Fig. 11e, f). In comparison, the wind event on March 21–22 (tide 21) also generated a strong undertow but a rather weak longshore current ($V=0.2$ m/s) because of the SW winds blowing with a lower incidence angle towards the coast. Therefore, mean flows in the surf zone were 2–3 times larger during wind-sea conditions than during even more energetic swell events ($U\approx0.15$ m/s, $V\approx0.2$ m/s at tide 7). Moderate wave conditions associated with strong winds blowing nearly parallel to the shoreline caused in consequence a large northward flux of sediments with all the sand eroded at the southern end of the beach being deposited downdrift over the high tide foreshore.

The occurrence of large wind speeds was accompanied by large fluctuations of the significant wave period at the tidal time scale (Fig. 11d). A detailed analysis of wave data in the spectral and temporal domains was undertaken (Fig. 12) to highlight the nature and origin of these large drops

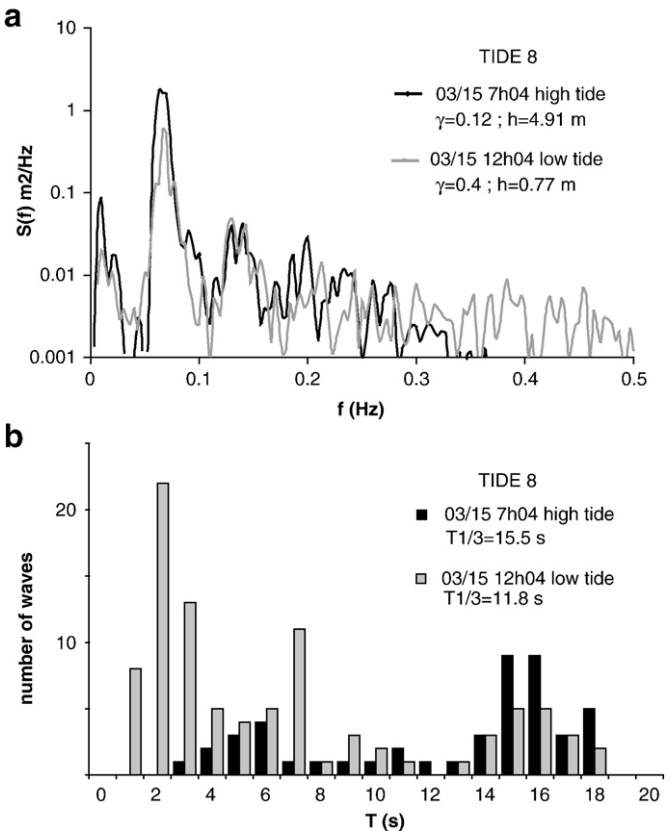

Fig. 12. (a) Wave energy spectra and (b) period of individual waves for consecutive high and low tides during a wind event at Corsen beach.

in the wave period signal between consecutive high and low tides. At the onset of the wind event (high tide 8; Fig. 12a), swell conditions still prevailed (peak frequency at 0.065 Hz). Energy seems to be present at harmonic frequencies (0.13 Hz, 0.2 Hz, 0.26 Hz) suggesting that part of the high frequency energy was related to bound waves generated by triad interactions at the peak frequency and between the harmonics themselves. Nonetheless, computed bispectra of sea surface elevation time series (not shown) lack a significant bicoherence at these particular frequencies, being noisy with a low bicoherence over all the frequency domain. Hence, we conclude that these high frequency waves were wind-induced. As the water depth decreased (end of falling tide, beginning of rising tide), energy was present in the entire high-frequency band (0.1–0.5 Hz) (Fig. 12a). The local strong wind blowing over the shallow foreshore generated very short sea waves ($T = 1$–4 s) (Fig. 12b) which became more and more predominant as swell activity lessened.

4.2.4. Infragravity waves

The conditions of formation of the sub-decimetric sand bar that appeared twice at the spring low tide levels (see Section 4.1) are examined. To do so, we took advantage of the position of the sand bar which coincided with the sensor location. Periods of efficient standing low water level during which the sand bar may have been formed were determined while the sensor was supposed to experience swash processes ($h < 0.3$ m and $\gamma_s > 0.3$; Fig. 13a) and in agreement with sand bar appearance at the spring low tide level. Both sand bar initiation events (March 23 and April 5–7) were associated with moderate wave conditions ($H_s = 0.3$–0.6 m) after a storm peak (Fig. 13b). At these periods, the amount of infragravity energy (in the whole 0–0.05 Hz band) was 9–47% of total wave energy in water depths of 13–30 cm, very close or even inside the swash zone (Fig. 13c). Swash processes were active at the spring low tide level for several tidal cycles (at least four) on April 5–7, resulting in increased sediment deposition and sand bar observation on April 8 (Fig. 6d). The duration of swash processes at the same beach level, on average 1–2 h per low tide and for several tidal cycles, the incident wave energy, and ensuing proportion of infragravity energy are the key parameters that control sand bar dynamics, from development to destruction.

Standing edge wave motions are also expected to be involved in beach cusp morphodynamics at Tregana Beach considering the semi-enclosed setting. Wave conditions during cusp initiation on May 25 and development (May 26 and following tides) were retrieved through a spectral analysis (Fig. 14 b–c). A subharmonic wave existed at a frequency of 0.05–0.06 Hz (half the primary wave frequency) as shown by a spectral peak. Therefore, a test of the theories involved in cusp formation was undertaken using the parameters reported in Table 4 applied to Eqs. (1)–(3). A comparison of observed and predicted cusp spacings at the time of their initiation (May 25 4h34 am) does not provide any clear evidence for the implication of either a standing edge wave or self-organized mechanisms in the cusp initiation process (Table 5). In fact, the self-organization theory underpredicts cusp spacing by around 8 m but the swash excursion has been evaluated making a number of strong assumptions with regards to the breaking wave height (Section 3.2). Also, we recall that cusp spacing may adjust not to the mean swash excursion but to the

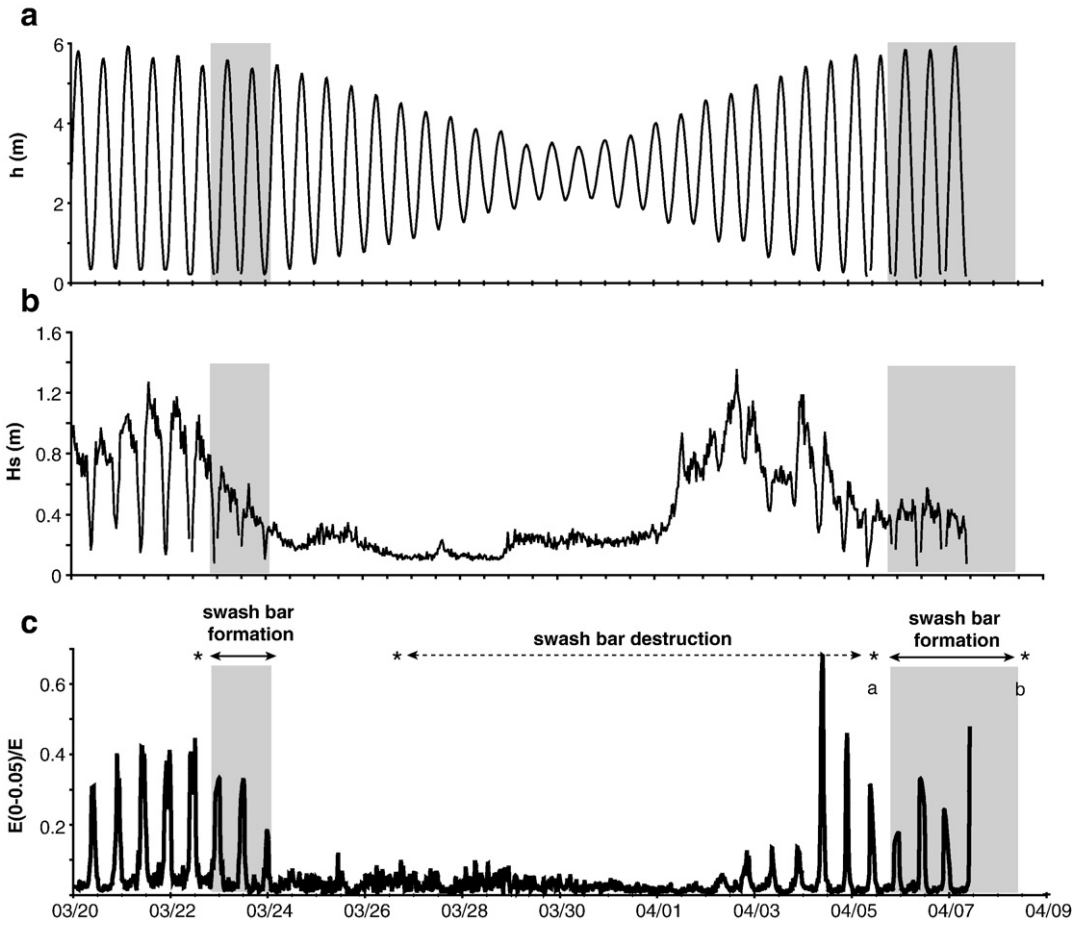

Fig. 13. Time series of water depth h, significant wave height Hs and ratio of energy in the whole infragravity band (0–0.05 Hz) to total energy. Stars refer to topographic surveys and grey bars to periods of swash bar formation.

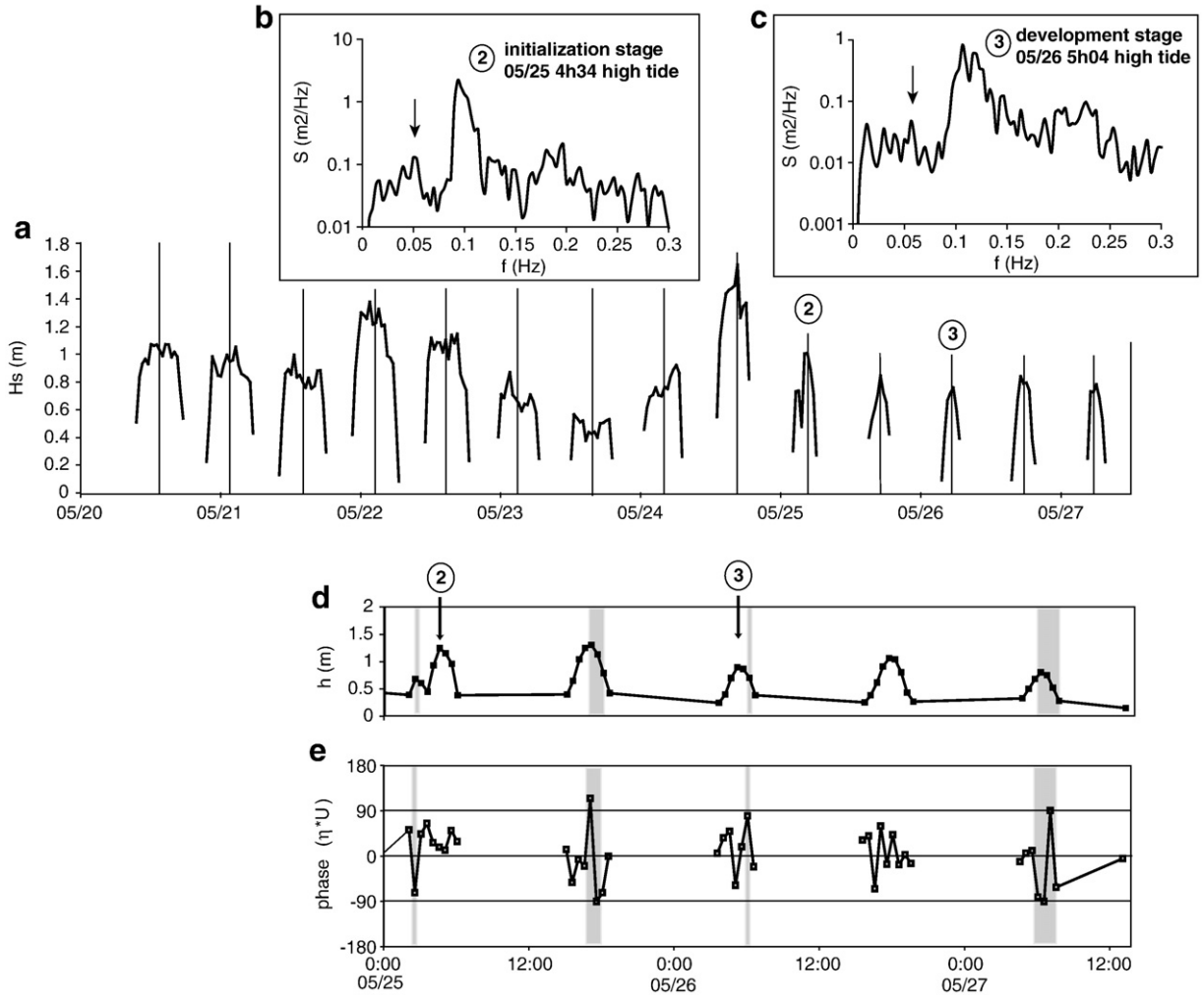

Fig. 14. (a) Time series of the significant wave height H_s, (b–c) wave energy spectra during cusp initiation and development (arrow indicates a peak at a sub-harmonic frequency); (d) water depth h above the sea bed; (e) phase relationship between the sea surface elevation and cross-shore flow speed signals in the frequency band 0.05–0.06 Hz (grey bars indicate occurrence of a standing sub-harmonic wave).

highest values (Ciriano et al., 2005). Finally, beach slope is quite tricky to estimate and a tiny difference could affect the spacing (but this argument is also valid for the edge wave predictions). Although the test of self-organization theory did not reveal any agreement between observed and predicted cusp spacing, the final topography (Fig. 7d) suggests swash zone morphodynamics to be three-dimensional with retroactive feedbacks between cusp morphology and swash currents (intermediate stage in the Masselink and Pattiaratchi, 1998a classification). Conversely, a relatively good agreement is reached between observed ($L_c = 23.5$ m) and predicted cusp spacing by the edge wave theory ($L_c = 21.7$–27.8 m) at the high tide levels during which cusp development occurred (May 26), not at the time of their initiation (May 25). In searching for signs of standing edge wave motions, phase relationships between sea surface elevation and cross-shore flow speed time series were then computed (Fig. 14e). We found that the subharmonic wave was standing at only two other high tides during which cusps developed (May 25 pm, May 27 am), once again not during their initiation.

5. Discussion

Our observations emphasize specificities in the hydrodynamics of pocket beaches, but also aspects of morphodynamic behaviour that are similar to those of their more open counterparts. These are discussed with reference to the following themes: (1) tidal currents, (2) wind forcing, (3) cross-shore and longshore sediment transport, (4) beach cusp formation, and (5) sand bar dynamics.

Table 4
Hydrodynamic and morphological parameters (spectral peak frequency f_p and period T_p, wave height at breaking H_b, swash length S, slope of the swash zone $\tan\beta_{swash}$) during initialization and development of the new cusps system (asterisk indicates a double spectral peak).

	f_p (Hz)	T_p (s)	H_b (m)	$\tan\beta_{swash}$	S (m)
05/25/05 4h34	0.093	10.7	1.0	0.107	9.3
05/26/05 5h04	0.106–0.12*	8.3*–9.4	0.72	0.101	7.15

Table 5
Observed and predicted beach cusp wavelength (in meter) according to standing edge wave theory and self-organization theory.

	L_c (obs.)	L_c (sub-harm.)	L_c (synchronous)	L_c (self-org.)
05/25/05 4h34	$23.5 \pm 0,7$	38.2	19.1	15.8
05/26/05 5h04	23.5 ± 0.7	21.7–27.8	10.8–13.9	12.1

5.1. Tidal currents

The results highlight a cross-shore variation in tidal currents from the intertidal to the subtidal zone. During non-breaking conditions, mean tidal currents are not significant in the intertidal zone (Fig. 10) whilst they are known to be strong off the pocket beaches (SHOM, 1994) and substantial $O(0.1–0.2$ m/s) in the subtidal zone of a wider embayed beach (Figs. 8 and 9). Such a gradient has never been reported across meso-macrotidal open beaches where tidal currents can be significant at least during low-energy wave conditions (for instance, Kroon and Masselink, 2002; Anthony et al., 2004; Sedrati and Anthony, 2007). We suggest that bedrocks and cliffs enclosing the beaches are geomorphological constraints that preclude the incursion of nearshore tidal currents onto the beachface.

5.2. Wind forcing

Contrary to what would be expected given the semi-enclosed setting, the role of wind forcing is crucial for pocket beach hydrodynamics by (1) superimposing short oblique waves onto the incident near-normal swells, or even by being the major forcing factor in areas protected from oceanic swells, and (2) stressing directly the water surface. It was actually demonstrated that the wind forcing alone can drive mean currents larger than those due to more energetic swells (Fig. 11), especially when winds blow nearly parallel to the beach. Even in areas exposed to oceanic swells, the mean longshore current reached a velocity greater than the undertow during storms (Fig. 10), and this was mainly ascribed to sidewise winds more than to incident swells. Therefore, local wind waves play a major role on pocket beaches independently of their degree of exposure to oceanic swells, driving strong mean flow motions, the undertow and the wind-induced longshore current. In terms of wind forcing, pocket beaches thus appear to be as much exposed as their more open counterparts (e.g., Reichmüth and Anthony, 2007; Sedrati and Anthony, 2007).

5.3. Cross-shore and longshore sediment transport

The geomorphological context (bounding headlands, embayed settings) confers on pocket beaches a certain ability to retain sediment despite relatively strong wind- and wave-induced currents during storms. Data from the beaches in Brittany show that the undertow efficiency in terms of net cross-shore sediment transport distance is rather weak, even during energetic wave conditions ($H_s = 1.2–1.4$ m), as outlined by the proximity of erosional and depositional areas which are separated by 30 m only (Fig. 6e). While the macrotidal range enables wave processes to move shoreward and then down the beachface with the water level variations, offshore sediment transport towards the subtidal zone occurs only during low tide levels, given the narrow surf zone. Thus, offshore sediment transport by the undertow is limited to the shoreface and very close to the upper subtidal beach during high-energy events. Moreover, even though the wind-induced longshore current is a major contributor to sediment transport during storms (Figs. 10, 11f), most sediments are trapped within the natural alongshore limits of the intertidal zone. As a result, pocket beaches deserve to be described as "sheltered beaches", first because of their moderate exposition to waves, but foremost due to their conservative sediment budget (weak sediment losses but also weak gains). They are thought to behave essentially with their own limited sand supply, recycling sediment from the nearshore to the shoreface (and vice versa) unlike open beaches which import (export) continuously sediment from the updrift (to the downdrift) end of the coastline. Nevertheless, sediment entering the system is still a possibility considering our results at intermediate depths (Fig. 9d) and those of previous studies which described both sediment resuspension and onshore flow motions induced by incident skewed waves under energetic swell conditions (Thornton et al., 1996; Ruessink et al., 1998; Storlazzi and Field, 2000; Storlazzi and Jaffe, 2002). Longshore sediment transport may occur over wider distances in the "large-scale" embayed system as soon as the surf zone extends beyond the rocky seabed, mainly during extreme storms. In addition, tidal currents may also drive alongshore sediment transport between adjacent pocket beaches bypassing rocky barriers, wave processes being finally in charge of the cross-shore sediment exchange. But it has also been suggested that the communication between adjacent pocket beaches is significantly controlled by the inner shelf underlying geology and bathymetry (e.g., Wright, 1987; Storlazzi and Field, 2000; Dolique and Anthony, 2005), an issue that is not addressed at all in this paper.

5.4. Beach cusp formation

Among the specificities relative to the hydrodynamics of pocket beaches that could lead to a particular change in beach morphology, we investigated the hypothesis of an alongshore standing edge wave developing at the shoreline that could force beach cusp generation. The analysis indicates standing edge waves to be possibly present only once cusps were formed, not at the time of their initiation (Fig. 14), which is the opposite of what theory would predict (Guza and Bowen, 1981) but in line with Bowen (1997) and recent observations (Ciriano et al., 2005) indicating more coherent infragravity activity once beach cusps were formed. Furthermore, the observed cusp spacing falls in the range of the numerous cusp systems surveyed along linear open beaches (review in Coco et al., 1999) while we would have expected the alongshore boundaries to force cusp spacing at a singular wavelength. We cannot conclusively refute any of the standing edge wave and self-organization hypotheses to explain beach cusp generation along pocket beaches because of limitations in the hydrodynamic measurements. Deployment of sensor arrays in the swash zone and video observations are needed (Özkan-Haller et al., 2001; Coco et al., 2003; Masselink et al., 2004; Almar et al., 2008) to resolve the spatial structure of the standing edge wave and detect evidence of self-organization processes.

5.5. Sand bar dynamics

Unlike the distinctiveness of certain hydrodynamic aspects of pocket beaches highlighted above, the intertidal sand bar morphodynamics of the pocket beaches in Brittany do not appear to be influenced by geomorphological constraints. As has been shown for open macrotidal beaches (Kroon and Masselink, 2002; Reichmüth and Anthony, 2007), the macrotidal range is a key factor in the behaviour of the intertidal beach by modulating, at the semi-diurnal neap-spring scale, the location and duration of wave processes. The observations from the pocket beaches of Brittany are in agreement with the general contention by Masselink et al. (2006) that the tide range (water depth over the bar) and the incident wave energy control together, the type, magnitude and duration of wave processes acting on the crest and seaward slope of the bar. Even for spring tide ranges (i.e., time periods during which the duration of wave processes on the bar is the shortest), a bar built up (Fig. 6) owing to the persistence of swash flow motions over several tidal cycles at the same level of the beach and under low energy conditions (Fig. 13). However, as soon as the water depth increased over the bar, swash processes could no longer operate, bar development ceased, and the bar was subject to breaking and surf zone motions (undertow and surf bores) that led to its early destruction. This is what happened to the swash bar formed on March 23, observed on March 26, which was subject to low-energy conditions until April 1, and then vanished under the action of storm waves (Fig. 13). Conversely, under persistent low-energy conditions, the sand bar should be able to maintain itself (even grow), and migrate onshore. Field observations during bimonthly beach surveys showed sand bars forming at neap high tide levels to move shoreward until forming a berm, and this was attributed to the rising neap-to-spring tidal ranges and to the associated displacement of swash zone processes (Dehouck, 2006). Our results are supported by the recent findings of Van Maanen et al. (2008) who showed onshore bar migration to occur at low tide when surf zone bores in very shallow water (<0.25 m) dominate the flow field.

6. Conclusions

This paper has reported a number of specificities of pocket beach hydrodynamics that have never been addressed before. First, a cross-shore variation in the velocity of mean tidal currents exists, "off" in the intertidal zone, "on" in the subtidal zone. Local geomorphological constraints, mainly due to bedrocks and cliffs bordering the beaches, isolate the shoreface from the active tidal circulation cell. Therefore, mean flow motions in the intertidal zone are exclusively wave-induced, and only active during energetic wind and wave events.

Secondly, the observed cross-shore and longshore mean currents attain velocities in the surf zone that are as strong as those along highly-exposed open beaches, despite fairly moderate wave energy conditions ($H_s = 0.8$–1.5 m during storms) and near-normal incident swells. Wind forcing is found to be as decisive in driving pocket beach hydrodynamics as along more widely open fetch-limited environments. The longshore current is mainly wind-driven with variations in velocity coherent with the wind direction relative to beach orientation. Furthermore, both cross-shore and longshore mean currents may be twice that observed during more energetic swell events (with larger H_s), especially when winds blow nearly parallel to the shoreline.

As along other macrotidal open environments, the tidal range is a key factor in controlling intertidal beach behaviour by modulating water level at the semi-diurnal neap-spring scale and thus the location and duration of wave shoaling, surf and swash processes over the shoreface. In particular, sand bar appearance at the spring low tide levels was shown to result from the action of swash processes at the same beach level during several tides and under post-storm wave conditions. Finally, the existence of a standing sub-harmonic edge wave over the beachface was demonstrated during beach cusp development but not at the precise time of their generation. Our present conclusions highlight the need for more detailed measurements to discriminate about the processes, edge waves and/or self-organization, forcing beach cusps formation along rocky coastlines.

Acknowledgements

Aurelie Dehouck benefited from a PhD grant from the French Ministry of Education and Research. Guy Amis, Alain Le Berre, Fabrice Ardhuin, David Corman, Patrice Bretel, Olivier Raynaud, Pierre Stephan are thanked for their constant assistance in the field and for sensor deployment; Veronique Cuq and Serge Suanez for beach surveying. Helene Howa, Giovanni Coco and the reviewers, Edward Anthony and Gerben Ruessink, are gratefully acknowledged for providing relevant comments and improving considerably the manuscript.

References

Aagaard, T., Black, K.P., Greenwood, B., 2002. Cross-shore suspended sediment transport in the surf zone: a field-based parameterization. Mar. Geol. 185 (3–4), 283–302.
Aagaard, T., Kroon, A., Andersen, S., Moller Sorensen, R., Quartel, S., Vinther, N., 2005. Intertidal beach change during storm conditions; Egmond, The Netherlands. Mar. Geol. 218 (1–4), 65–80.
Almar, R., Coco, G., Bryan, K.R., Huntley, D., Short, A.D., Sénéchal, N., 2008. Video observations of beach cusp morphodynamics. Mar. Geol. 254 (3–4), 216–223.
Anthony, E.J., Levoy, F., Monfort, O., 2004. Morphodynamics of intertidal bars on a megatidal beach, Merlimont, Northern France. Mar. Geol. 208 (1), 73–100.
Baldock, T.E., Holmes, P., 1999. Simulation and prediction of swash oscillations on a steep beach. Coast. Eng. 36, 219–242.
Bowen, A.J., 1997. Patterns in the water, patterns in the sand? Proceedings 3rd International Conference on Coastal Dynamics. ASCE, pp. 1–10.
Castelle, B., Bonneton, P., Senechal, N., Dupuis, H., Butel, R., Michel, D., 2006a. Dynamics of wave-induced currents over an alongshore non-uniform multiple-barred sandy beach on the Aquitanian Coast, France. Cont. Shelf Res. 26 (1), 113–131.
Castelle, B., Bonneton, P., Butel, R., 2006b. Modélisation du festonnage des barres sableuses d'avant-côte: application à la côte aquitaine, France. C. R. Geosci. 338, 795–801.
Ciriano, Y., Coco, G., Bryan, K.R., Elgar, S., 2005. Field observations of swash zone infragravity motions and beach cusp evolution. J. Geophys. Res. 110, C02018.
Coco, G., Murray, A.B., 2007. Patterns in the sand: from forcing templates to self-organization. Geomorphology 91, 271–290.
Coco, G., O'Hare, T.J., Huntley, D.A., 1999. Beach cusps: a comparison of data and theories for their formation. J. Coast. Res. 15 (3), 741–749.
Coco, G., Huntley, D.A., O'Hare, T.J., 2000. Investigation of a self-organisation model for beach cusps formation and development. J. Geophys. Res. 105 (C9), 21991–22002.
Coco, G., Burnet, T.K., Werner, B.T., Elgar, S., 2003. Test of self-organization in beach cusp formation. Journal of Geophysical Research 108 (C3), 3101.
Costas, S., Alejo, I., Vila-Concejo, A., Nombela, M.A., 2005. Persistence of storm-induced morphology on a modal low-energy beach: a case study from NW-Iberian Peninsula. Mar. Geol. 224, 43–56.
Dehouck, A., 2006. Morphodynamique des plages sableuses de la mer d'Iroise (Finistère). PhD thesis, Université de Bretagne Occidentale, pp. 262.
Dehouck, A., Seube, N., Suanez, S., Cuq, V., Howa, H., 2007. Variabilité cross-shore d'une plage de poche macrotidale: dynamique saisonnière, profondeur de fermeture, bilan de matière et disponibilité sédimentaire. Proceedings 11ème Congrès français de sédimentologie, Caen, France, book of abstracts, p. 1.
Dolique, F., Anthony, E.J., 2005. Short-term profile changes of sandy pocket beaches affected by Amazon-derived mud, Cayenne, French Guiana. J. Coast. Res. 21 (6), 1195–1202.
Falqués, A., Coco, G., Huntley, D.A., 2000. A mechanism for the generation of wave-driven rhythmic patterns in the surf zone. J. Geophys. Res. 105 (C10), 24071–24088.
Garcez Faria, A.F., Thornton, E.B., Lippmann, T.C., Stanton, T.P., 2000. Undertow over a barred beach. J. Geophys. Res. 105 (C7), 16999–17010.
Goodfellow, B.W., Stephenson, W.J., 2005. Beach morphodynamics in a strong-wind bay: a low-energy environment? Mar. Geol. 214, 101–116.
Greenwood, B., Osborne, P.D., 1990. Vertical and horizontal structure in cross-shore flows: an example of undertow and wave set-up on a barred beach. Coast. Eng. 14 (6), 543–580.
Guza, R.T., Bowen, A.J., 1981. On the amplitude of beach cusps. J. Geophys. Res. 86 (C5), 4125–4132.
Guza, R.T., Inman, D.L., 1975. Edge waves and beach cusps. J. Geophys. Res. 80 (21), 2997–3012.
Hallermeier, R.J., 1981. A profile zonation for seasonal sand beaches from wave climate. Coast. Eng. 4, 253–277.
Holman, R.A., Bowen, A.J., 1982. Bars, bumps and holes: models for the generation of complex beach topography. J. Geophys. Res. 87 (C1), 457–468.
Holman, R.A., Symonds, G., Thornton, E.B., Ranasinghe, R., 2006. Rip spacing and persistence on an embayed beach. J. Geophys. Res. 111, CO1006.
Horn, D.P., 1993. Sediment dynamics on a macrotidal beach: Isle of Man, U.K. J. Coast. Res. 9 (1), 189–208.
Huntley, D.A., Bowen, A.J., 1978. Beach cusps and edge waves. Proceedings 16th International Conference on Coastal Engineering. ASCE, New York, pp. 1378–1393.
Inman, D.L., Guza, R.T., 1982. The origin of swash cusps on beaches. Mar. Geol. 49, 133–148.
Jackson, N.L., Nordstrom, K.F., Eliot, I., Masselink, G., 2002. 'Low energy' sandy beaches in marine and estuarine environments: a review. Geomorphology 48 (1–3), 147–162.
Kim, Y.C., Powers, E.J., 1979. Digital bispectra analysis and its application to nonlinear wave interactions. IEEE Trans. Plasma Sci. 7 (2), 120–131.
Kroon, A., Masselink, G., 2002. Morphodynamics of intertidal bar morphology on a macrotidal beach under low-energy wave conditions, North Lincolnshire, England. Mar. Geol. 190 (3–4), 591–608.
Levoy, F., Monfort, O., Larsonneur, C., 2001. Hydrodynamic variability on megatidal beaches, Normandy, France. Cont. Shelf Res. 21 (6–7), 563–586.
Masselink, G., 1993. Simulating the effects of tides on beach morphodynamics. J. Coast. Res., SI 15, 180–197.
Masselink, G., Black, K.P., 1995. Magnitude and cross-shore distribution of bed return flow measured on natural beaches. Coast. Eng. 25 (3–4), 165–190.
Masselink, G., Pattiaratchi, C.B., 1998a. Morphological evolution of beach cusps and associated swash circulation patterns. Mar. Geol. 146 (1–4), 93–113.
Masselink, G., Pattiaratchi, C.B., 1998b. The effect of sea breeze on beach morphology, surf zone hydrodynamics and sediment resuspension. Mar. Geol. 146 (1–4), 115–135.
Masselink, G., Short, A.D., 1993. The effect of tide range on beach morphodynamics and morphology: a conceptual beach model. J. Coast. Res. 9 (3), 785–800.
Masselink, G., Russell, P., Coco, G., Huntley, D., 2004. Test of edge wave forcing during formation of rhythmic beach morphology. J. Geophys. Res. 109, C06003.
Masselink, G., Kroon, A., Davidson-Arnott, R.G.D., 2006. Morphodynamics of intertidal bars in wave-dominated coastal settings — a review. Geomorphology 73 (1–2), 33–49.
Oltman-Shay, J., Guza, R.T., 1987. Infragravity edge wave observations on two California beaches. J. Phys. Oceanogr. 17, 644–663.
Osborne, P.D., Greenwood, B., 1992. Frequency dependent cross-shore suspended sediment transport: 2. A barred shoreface. Mar. Geol. 106, 25–51.
Özkan-Haller, H.T., Vidal, C., Losada, I.J., Medina, R., Losada, M.A., 2001. Standing edge waves on a pocket beach. J. Geophys. Res. 106 (C8), 16981–16996.
Pattiaratchi, C., Hegge, B., Gould, J., Eliot, I., 1997. Impact of sea-breeze activity on nearshore and foreshore processes in southwestern Australia. Cont. Shelf Res. 17 (13), 1539–1560.
Price, T.D., Ruessink, B.G., 2008. Morphodynamic zone variability on a microtidal barred beach. Mar. Geol. 251, 98–109.
Raubenheimer, B., Guza, R.T., Elgar, S., 1996. Wave transformation across the inner surf zone. J. Geophys. Res. 101 (C10), 25589–25597.
Reichmüth, B., Anthony, E.J., 2007. Tidal influence on the intertidal bar morphology of two contrasting macrotidal beaches. Geomorphology 90, 101–114.
Ruessink, B.G., Houwman, K.T., Hoekstra, P., 1998. The systematic contribution of transporting mechanisms to the cross-shore sediment transport in water depths of 3 to 9 m. Mar. Geol. 152 (4), 295–324.
Sedrati, M., Anthony, E.J., 2007. Storm-generated morphological change and longshore sand transport in the intertidal zone of a multi-barred macrotidal beach. Mar. Geol. 244, 209–229.

Sénéchal, N., Dupuis, H., Bonneton, P., Howa, H., Pedreros, R., 2001. Observation of irregular wave transformation in the surf zone over a gently sloping sandy beach on the French Atlantic coastline. Oceanol. Acta 24 (6), 545–556.
Sénéchal, N., Rey, V., Bonneton, P., Dupuis, H., 2005. On the difficulty of correctly determine the characteristic wave period in the surf zone. Proceedings 5th International Conference on Coastal Dynamics. ASCE, New York, p. 12.
SHOM, 1994. Courants de marée de la côte ouest de Bretagne de Goulven à Penmarc'h.
Short, A.D., 1991. Macro-meso tidal beach morphodynamics — an overview. J. Coast. Res. 7 (2), 417–436.
Storlazzi, C.D., Field, M.E., 2000. Sediment distribution and transport along a rocky, embayed coast: Monterey Peninsula and Carmel Bay, California. Mar. Geol. 170, 289–316.
Storlazzi, C.D., Jaffe, B.E., 2002. Flow and sediment suspension events on the inner shelf of central California. Mar. Geol. 181, 195–213.
Thornton, E.B., Humiston, R.T., Birkemeier, W., 1996. Bar/through generation on a natural beach. J. Geophys. Res. 101 (C5), 12097–12110.
Turner, I., Whyte, D., Ruessink, B.G., Ranasinghe, R., 2007. Observations of rip spacing, persistence and mobility at a long, straight coastline. Mar. Geol. 236, 209–221.
van Enckevort, I.M.J., Reincke, E., 1996. Longshore currents in the intertidal zone of Terschelling. IMAU Report V96.09. Utrecht University, The Netherlands, p. 62.
Van Maanen, B., de Ruiter, P.J., Coco, G., Bryan, K.R., Ruessink, B.G., 2008. Onshore sandbar migration at Tairua Beach (New Zealand): numerical simulations and field measurements. Mar. Geol. 253 (3–4), 99–106.
Werner, B.T., Fink, T.M., 1993. Beach cusps as self-organized patterns. Science 260, 968–971.
Wijnberg, K.M., Kroon, A., 2002. Barred beaches. Geomorphology 48 (1–3), 103–120.
Wright, L.D., 1987. Shelf — surf zone coupling: diabatic shoreface transport. Proceedings International Conference on Coastal Sediments. ASCE, New York, pp. 25–40.
Wright, L.D., Short, A.D., 1984. Morphodynamic variability of surf zones and beaches: a synthesis. Mar. Geol. 56, 93–118.